MODELING OF OVERALL HEAT TRANSFER COEFFICIENT OF A CONCENTRIC DOUBLE PIPE HEAT EXCHANGER WITH LIMITED EXPERIMENTAL DATA BY USING CURVE FITTING AND ANN COMBINATION

by

Necati KOCYIGIT [*] ***and Huseyin BULGURCU***
Konukisi Consultant, Basaksehir, Istanbul, Turkey

Original scientific paper
https://doi.org/10.2298/TSCI171206111K

The modeling accuracy of artificial neural networks (ANN) was evaluated by using limited heat exchanger data acquired experimentally. The artificial neural networks were used for predicting the overall heat transfer coefficient of a concentric double pipe heat exchanger where oil flowed inside the inner tube while the water flowed in the outer tube. In the cases of parallel and counter flows, the experimental data were collected by testing heat exchanger in wide range of operating conditions. Curve fitting and artificial neural network combination was used for the estimation of the overall heat transfer coefficient to compensate the experimental errors in the data. The curve fitting was used to detect the trend and generate data points between the experimentally collected points. The artificial neural network was trained better from the generated data set. The feed forward type artificial neural network was trained by using the Levenberg-Marquardt algorithm. Two backpropagation network type artificial neural network algorithms were also used, and their performance were compared with the estimation of the Levenberg-Marquardt algorithm. The average estimation error between the predictions and the experimental data were in the range of 1.31e–4 to 4.35e–2%. The study confirmed that curve fitting and artificial neural network combination could be used effectively to estimate the overall heat transfer coefficient of heat exchanger.

Key words: *modeling, overall heat transfer coefficient, curve fitting, artificial neural network*

Introduction

Over the last decades, heat exchangers (HX) have become increasingly important because of their rules in energy conservation, recovery, conversion, and implementation of new energy sources. The HX are widely used in air-conditioning and refrigeration, power, transportation, alternative fuels, heat recovery, cryogenic, and manufacturing industries, as well as being key components of many industrial products available in the marketplace. Although significant advances have taken place in the development of HX manufacturing technology as well as design theory [1-4], new industrial challenges require further research in HX analysis, particularly using advanced methodologies, such as artificial neural networks (ANN).

The ANN have been applied in modeling heat transfer phenomena of different HX applications because of its ability in providing better and more reasonable solutions [5, 6]. Pacheco-Vega *et al.* [7] predicted the performance of fin-tube HX and air-water HX using

* Corresponding author, e-mail: dr.necati.kocyigit@gmail.com

ANN. Mohanraj *et al.* [8] reviewed the application of ANN for thermal analysis of HX. The use of ANN-based neuro-controllers in HX is a recently developed field. Díaz *et al.* [9] reported dynamic prediction and control of HX using ANN. Esfe [10] has applied the post-processing of experimental data on the flow and heat transfer in a nanofluid-based double tube heat exchanger using an ANN. Naphon *et al.* [11] have studied on the application of ANN to analyze the heat transfer and friction factor of the horizontal double tube HX with spring insert. Fadare and Fatona [12] developed an ANN model for modeling the overall heat transfer coefficient of a staggered multi-row, multi-column, cross-flow, tube-type HX. Islamoglu [13] developed an ANN model for predicting the suction line outlet temperature and mass flow rate of a capillary tube suction line HX used in household refrigerators. Shabiulla and Sivaprakasam [14] have conducted experiments by using cold fluid (Butanol) and hot fluid (water) in constant mass--flow rate of hot fluid and they have proposed ANN models for the analysis of a spiral plate HX. Xie *et al.* [15] set up an experimental system for investigation on performance of shell-and-tube HX and obtained limited experimental data. They predicted temperature differences and heat transfer rate for HX using the ANN. Colorado *et al.* [16] designed a physical-empirical model to describe heat transfer of helical coil in oil and glycerol/water solution. Patra *et al.* [17] have designed and developed an ANN model for process modelling of intermediate HX subsystem in nuclear reactor.

Several investigators have also focused on some research on HX. Erdogan and Colpan [18] assessed the effect of the source temperature on the performances of the shell and tube heat exchanger and the organic Rankine cycle. Ali *et al.* [19] observed that this design feature of a counter-flow heat and mass exchanger can lead to a substantial increase of dew-point and wet-bulb effectiveness. Direk and Kelesoglu [20] presented the energy and exergy analysis of an R1234yf automotive air conditioning system. For this aim, an experimental baseline an automobile air conditioning system was developed and a double pipe internal HX was employed to the system.

Curve fitting (CF) regression analysis is used to find the best fit of curve for a series of data points. The curve fit generally produces an equation that can be used to find points anywhere along the curve. Because the experimental data always contains error, it is required to fit the data as well as possible. The CF is performed to fit data sets that contain outliers.

In recent researches, some CF were applied to the experimental data for the best fit of curve for a set of data points. The CF was applied to the performance of heat pump determined by manufacture's catalog data [21]. The CF was applied to experimental data of shell tube HX [22]. Mathematical information of relation between optimum exergy efficiency and the total length of the system was given by the fitted curve [23].

During experimentally the tests, some errors in the acquired data were likely to deteriorate the prediction performance of the developed model. Thus, we proposed CF and ANN combination to represent the experimental data when only limited number of readings were available. For better results of calculation, some correlations in good estimating confidence intervals for the optimal result of input values were performed by using CF. Otherwise, lack of the acquired data may lead to cause poor performance of the ANN model. Sufficient data were generated for better training and testing with the help of correlations.

A concentric double pipe oil to water HX was used for modeling of overall heat transfer coefficient. The goal of this study is to estimate the overall heat transfer coefficient, U, of the heat changer using CF and ANN combination. For this aim, an experimental set-up was developed. Unlike similar ones, HX is fixed to the experimental set-up with 45° inclination. The oil inlet and outlet temperatures, water inlet and outlet temperatures, and water mass flow rate were

used as the input data of the ANN model, while the U was used as the output of the model. Each flow mode was performed separately by using three ANN algorithms and the obtained results were compared with the experimental values.

Theoretical background

Types of flow configuration

The HX transfer heat between two or more streams of fluid that flow through the equipment. A major characteristic of HX design is the relative flow configuration, which is the set of geometric relationships between the streams.

It must be accentuated that the configurations described represent idealizations of what truly occurs. In practice, it is never possible to make the flow patterns comply to the ideal. In a counter-flow heat exchanger, the two fluids flow parallel to each other in opposite directions.

Curve fitting and ANN modeling

Because experimental data always contain error, connecting the dots on a graph is not commonly preferred. Instead of connecting the dots on a graph, CF is used to find the best fit of line or curve for a series of data points. The curve fit generally produces an equation that can be used to find points anywhere along the curve [24].

The ANN comprise a multiple layers, which are termed input, hidden, and output layer, respectively. These layers consist of input nodes, hidden nodes, and output node(s), respectively [25]. The characteristics of the systems may be modeled by using CF methods and ANN methods evaluate the parameters of a theoretical or empirical equation. The ANN use the same generic equation to represent the characteristics of any system without demanding any models. The experimentally collected concentric double pipe heat exchanger data was modeled by use of ANN.

The author previously implemented a resilient backpropagation (RB), a scaled conjugate gradient backpropagation (SCG), and a Levenberg-Marquardt (LM) algorithm to estimate the faulty conditions of the vapor compression refrigeration system [26]. In this study, the same three types of ANN algorithms were used to model the considered system.

Description of the experimental set-up and testing procedure

In this study, an experimental set-up was developed for data generation. The experimental set-up consisted of a heater tank, a HX, a circulation pump, a bypass and flow control valve, a proportional integral derivative (PID) controller with resistance temperature detector (RTD) and a flow meter. The HX was fixed to the experimental set-up with 45° inclination. In addition, temperature measurements at 4 points were performed on the set-up. The schematic diagram of the experimental set-up is shown in fig. 1.

The components of the experimental set-up are explained: (a) *heat exchanger*: A concentric double pipe HX has been designed with the goal of accomplishing maximum heat transmission at minimum pressure drop. The outer spiral-formed space leads water in a flow counter to the flow of oil in the inner space. Built into the inner space are offset fin sections [27]. The HX was manufactured from brass and copper, and has very small dimensions in relation to its heat transmission capacity. The spiral formed outer space forces the hot refrigerant liquid over the entire heat transmission surface and prevents the formation of condensate on the outer space. The built-in offset fin sections in the inner space produce turbulent flow in the refrigerant vapor. Thus, the heat transmission from liquid to vapor is very effective. At the same time,

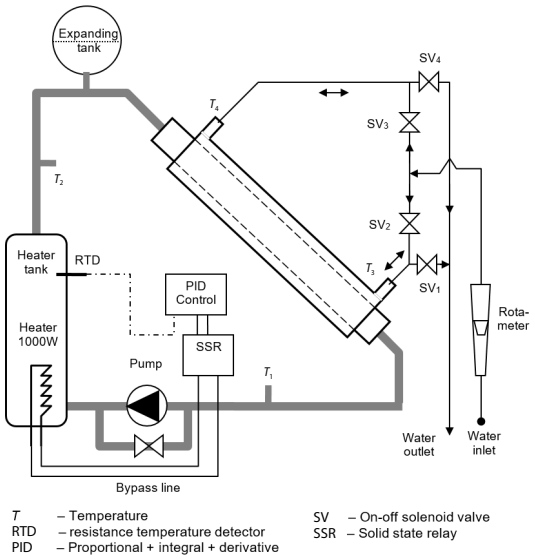

Figure 1. Schematic diagram of the laboratory type HX unit

Table 1. Characteristics of the HX

Characteristic	Value
Weight, [kg]	1.692
Outer diameters of tubes, [mm]	41.3
Wall thickness of tubes, [mm]	1.27
Tube length, [mm]	310
Inlet size, [mm]	28
Max. Working Pressure, [bar]	21.5
Outlet size, [mm]	12

pressure drop is kept down to a reasonable level. The detail of the HX is given in tab. 1.

This HX was manufactured for the liquid-vapor lines of refrigeration systems. (b) *heater:* The electric resistance type heater is placed near the bottom side of a steel tank, and has a capacity of 1000 W. (c) *PID controller:* Heater is controlled by a PID temperature controller using SSR. It has self-tuning feature. (d) *temperature sensor:* A RTD is used as a temperature sensor (PT100), and it is located in the middle of the heater tank. (e) *circulation pump:* The pump has 5.6 mH_2O head pressure, and 3.4 m^3/h flow rate. (f) *multi temperature selector and display:* Oil inlet and outlet temperatures, where are located at the oil inlet (point 1) and outlet (point 2) of the heater tank, are measured by RTD type sensor. Water inlet and outlet temperatures, where located at the inlet (point 3), and outlet (point 4) of the HX water line, are measured by NTC type thermistors. Some features of the instrumentation are summarized in tab. 2.

The ANN modeling approach for parallel flow and counter flows has been applied to the experimental set-up shown in fig. 1. The oil is pumped into the central tube and comes in contact with the counter-flowing water, which is supplied from the city water line into the annular space. The oil is heated by electric resistance and its temperature is controlled by PID controller and a SSR. A control valve is provided to adjust the flow rate of the water. Various transport properties of the oil is given in tab. 3. Measurements were taken in the range of 100 L/h to 500 L/h with 20 L/h increments. In the experimental study, totally 21 different steady-state test runs for parallel flow and counter flow have been conducted to gather data for training the proposed ANN model and testing its performance. The ranges of measured variables for parallel flow and counter flows are shown in tab. 4.

Data generation and ANN modeling

Due to measurement errors, the acquired data had error. The accuracy of the data was improved by using the CF method which reduced the errors by smoothing the curve. This

Table 2. Characteristics of the instrumentation

Measured variable	Instrument	Range	Accuracy
Oil temperature, [ºC]	RTD type sensor	–50 to 200	0.3 ºC
Water temperature, [ºC]	NTC type thermistor	–20 to 100	0.2 ºC
Water mass-flow rate, [Lh^{-1}]	Variable area flow meter	50-500	5%

Table 3. Transport properties of oil

Transport properties	Test standards	Value
Density, at 20 °C, [kgm^{-3}]	DIN 51757	0.869
Viscosity, at 40 °C,[mm^{2}s^{-1}]	DIN 51562	33
Flame point, [ºC]	DIN 51584	220
Working temperature, [ºC]		350
Specific heat, at 45 °C, [kJkg^{-1}K^{-1}]		1.977
Thermal conductivity, [Wm^{-1}K^{-1}]		0.12
Freezing point, [ºC]	ISO 3016	–16
Boiling point, [ºC]	DIN 51582/ISO 3733	360

Table 4. Range of measured variables in the experiments for parallel flow and counter flows

Measured variable	Instrument	Parallel flow	Counter flow
Oil input temperature, [ºC]	RTD type sensor	55.7-45.3	52.3-42. 8
Oil output temperature, [ºC]	RTD type sensor	55.8-45.9	52.5-43.3
Water input temperature, [ºC]	NTC type thermistor	15.2-13.8	15.2-13.7
Water output temperature, [ºC]	NTC type thermistor	25.5-15.9	24.4-15.6
Water mass-flow rate, [Lh^{-1}]	Variable area flow meter	100-500	100-500

approach reduces the possible ANN representation errors when the number of hidden nodes is increased. To fix or reduce errors in experimental data, CF equations of polynomial and exponential series models were used to do the best fit of data.

The CF equation of polynomial series [28], *y,* in a single indeterminate can be expressed:

$$y = \sum_{i=1}^{n+1} p_i x^{n+1-i} \tag{1}$$

where i, n, p, and x are iteration number, number of term in the series, constant value, and variable respectively.

Water input data, $T_{c,in}$, and output data, $T_{c,out}$, for counter flow were calculated by using polynomial eq. (1) with third degree and with fourth degree, respectively. However, for parallel flow they were calculated by using equationd with third and first degree, respectively. The best fit of $T_{c,in}$ and $T_{c,out}$ for counter and parallel flows were acquired. Oil input data, $T_{h,in}$, and output data, $T_{h,out}$, for parallel flow were calculated by using a polynomial equations with fourth degree. However for parallel flow, they were calculated by using with first degree, and the best fit of $T_{h,in}$ and $T_{h,out}$ was acquired. Water mass-flow rate, $\dot{m}_w$, was calculated by using a polynomial equation with first degree and the best fit of $\dot{m}_w$ was acquired.

After acquiring data by using calculations, the logarithmic mean temperature difference (LMTD) method was tested to calculate the overall heat transfer coefficient, U. This methods can be explained as follows [2-4].

Because the temperature difference between the oil, T_h, and water, T_c, streams varies along the length of the concentric double pipe HX, it is essential to derive an average temperature difference from the heat transfer calculations.

Let T_h and T_c, respectively, denote the temperature of the hot and cold fluids. Furthermore, let ΔT_1 and ΔT_2 stand for the temperature difference at each terminal side of the HX, *i. e.*,

$$\Delta T_1 = \begin{cases} T_{h,in} - T_{c,out} & \text{if counter flow,} \\ T_{h,in} - T_{c,in} & \text{if parallel flow} \end{cases} \tag{2}$$

$$\Delta T_2 = \begin{cases} T_{h,out} - T_{c,in} & \text{if counter flow,} \\ T_{h,out} - T_{c,out} & \text{if parallel flow} \end{cases} \tag{3}$$

where $T_{c,in}$ and $T_{c,out}$ are input and output temperatures of the cold fluid and $T_{h,in}$ and $T_{h,out}$ are input and output temperatures of the hot fluid respectively.

The LMTD can be calculated from:

$$\Delta T_m = \frac{\Delta T_2 - \Delta T_1}{\ln \dfrac{\Delta T_2}{\Delta T_1}} \tag{4}$$

with T_1 and T_2 as defined in eqs. (2) and (3).

U can be calculated:

$$U = \frac{\dot{Q}_e}{A_s \Delta T_m} \tag{5}$$

where $\dot{Q}_e$ is heat transfer rate which is emitted from hot liquid and A_s is heat transmission area.

Followings are the assumptions made in the thermal analysis of heat exchanger by LMTD:

- U is constant over the length of fluid.
- The specific heat is constant over entire length of path.
- There are no partial phase changes in the system.
- Heat losses to the surrounding air are negligible because pipe, heater tank and circulation pump are insulated by rockwool.

After acquiring and calculating all necessary data, the network architecture of CF and ANN model has been applied to predict optimal results of the counter flow and the parallel flow for the overall heat transfer coefficient, U. Input nodes which are oil input temperature, $T_{h,in}$, oil output temperature, $T_{h,out}$, water input temperature, $T_{c,in}$, water output temperature, $T_{c,out}$, and water mass-flow rate, $\dot{m}_w$, were used and output node which is the overall heat transfer coefficient, U, was used. The different number hidden nodes were used to predict an optimal result of counter and parallel mass-flow rates.

The performance of the ANN is evaluated by assessing the estimation errors on the training data. Then, the estimation error on the testing data is recalculated after the ANN predicts the output(s). The estimation errors on the testing data are generally higher compared to the training data. Respect to range of target data, average percentage error of every predicted output of training and testing data was defined:

$$R_{ave} = \frac{1}{N} \frac{\sum_{i=0}^{n} \left| A^e - A^p \right|}{\left| A^e_{max} - A^e_{min} \right|} \tag{6}$$

where A^e is the experimental data, A^p is the predicted result, and N is the number of data. The network architecture of this ANN model with CF is shown in fig. 2.

Furthermore, one-way ANOVA were employed for determining the means of groups. The ANOVA uses *F*-statistic to statistically test the equality of means. The *F*-statistic simply a ratio of the mean squared errors. The sources of variance on experimental values of the two or more groups can be separated into constituent parts and accurately measured. The ANOVA returns to the *p*-value for a balanced one-way ANOVA by group. The *p*-value is the probability that the test statistic may take a value greater than the value of the computed test statistic [29].

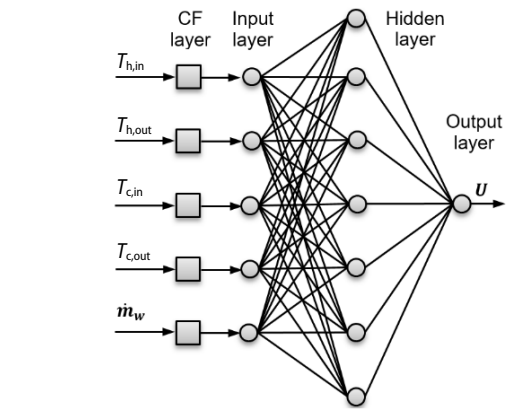

$T_{h,in}$ Input temperature of hot fluid
$T_{h,out}$ Output temperature of hot fluid
$T_{c,in}$ Input temperature of cold fluid
$T_{c,out}$ Output temperature of cold fluid
$\dot{m}_w$ Mass flow rate of water
CF Curve fitting
U Heat transfer coefficient

Figure 2. Network architecture of CF and ANN model

Limitations of ANN modeling for HX and uncertainty analysis

The major limitations of ANN for HX analysis consist of over training errors, extrapolation errors and optimization of network configuration [30]. In this study, the network consisted of one input layer with 5 neurons, one hidden layer, and one output layer with one node, fig. 2. The number of hidden nodes increased from 1 to 40. The LM, RB, and SCG type ANN were trained and tested by using the generated data. The LM had the best estimations in all the cases after 40 trials and 1000 training iterations for each cases when the results of estimating errors were compared. For compact representation and consistency, the LM type ANN with 8 hidden nodes was selected. Due to the best performance, the LM type ANN was selected to represent ANN. The ANN parameters for LM type ANN were shown in tab. 5.

The uncertainty analysis for the overall heat transfer coefficient, *U*, for the counter and parallel flows was performed using by Moffat in [31]. According to this method, the function, *R,* is presumed to be computed from a set of the totally *N* measurements represented:

$$R = R\left(m_1, m_2, m_3, \ldots, m_N\right) \tag{7}$$

Then the uncertainty of the result *R* can be calculated:

$$\delta R = \sqrt{\sum_{i=1}^{N}\left(\frac{\partial R}{\partial m_i}\delta m_i\right)^2} \tag{8}$$

Using the accuracies for the measured variables denoted in tab. 2, the uncertainty of the calculated *U* was determined with the evaluation of eq. (7) in eq. (8). The total uncertainty of *U* for the counter and parallel flows was 6.95% and 6.18%, respectively.

Results and discussion

In this section, the characteristics of the data and the need for CF will be discussed. Next, the empirical model for representation of the experimental data was introduced. Then,

Table 5. Neural network parameters for LM type ANN

Parameter	Value	Description
net.trainParam.epochs	1000	Maximum number of epochs
net.trainParam.goal	0	Performance goal
net.trainParam.max_fail	1000	Maximum validation failures
net.trainParam.min_grad	1e–20	Minimum performance gradient
net.trainParam.mu	0.001	Initial mu
net.trainParam.mu_dec	0.1	mu decrease factor
net.trainParam.mu_inc	10	mu increase factor
net.trainParam.mu_max	1e20	Maximum mu
net.trainParam.show	25	Epochs between displays
net.trainParam.time	inf	Maximum time to train in seconds

data generation for training of the ANN will be outlined. Finally, the performance of the ANN will be discussed.

Experimental data were collected with parallel flow and counter flow studies. Measurements were taken in the range of 100 L/h to 500 L/h with 20 L/h increments. Therefore, 21 different measurements were taken in each case (mode). The U for parallel and counter flows was calculated by the LMTD method. The calculated U for the parallel flow was in range of 297.683 to 309.906. However, for the counter flow the calculated U was in range of 324.365 to 369.228. The ANN had one input layer with 5 nodes, one hidden layer, and one output layer with single node. The LM, SCG, and RB type ANN were trained with 14 cases while the number of hidden nodes was increased from 1 to 40. The performances of the ANN were evaluated by using the 7 cases which they never saw before. The average estimation percentage errors, R_{ave}, without CF for testing were in the range of 31.1% to 0.75% when the LM type of ANN was used. Due to measurement errors, the acquired data had error. The accuracy of the data was improved by using the CF method which reduced the errors by smoothing the curve. This approach reduces the possible ANN representation errors when the number of hidden nodes is increased.

Secondly, sufficient data was generated by CF for better training of the ANN. Polynomial series models were used to fit a curve to the experimental data and to generate the training cases for the ANN. The curves generated by the empirical models were always within the 95% confidence bounds of the data. The water input, $T_{c,in}$, temperatures for counter flow were derived from eq. (1) with third degree. However the water output, $T_{c,out}$, were derived from eq.(1) with fourth degree. The R^2 of $T_{c,in}$ and $T_{c,out}$ were 0.9996 and 0.9993, respectively. Water input, $T_{c,in}$, temperatures for parallel flow were derived eq. (1) with third degree. But, the water output, $T_{c,out}$, were derived from eq. (1) with one term. The R^2 of $T_{c,in}$ and $T_{c,out}$ were 0.9986 and 1, respectively. Oil input, $T_{h,in}$, and output, $T_{h,out}$, temperature for the counter flow were derived from the polynomial equation with fourth degree and R^2 of $T_{h,in}$ and $T_{h,out}$ were 0.9992 and 0.9991 respectively. However, oil input, $T_{h,in}$, and output, $T_{h,out}$, temperatures of parallel flow were derived from the polynomial equation with one term. The R^2 of $T_{h,in}$ and $T_{h,out}$ were 0.9993 and 0.9983 respectively. The mass-flow rate of water was derived from polynomial equation, and R^2 of $\dot{m}_w$ was 1.

Third, the performances of the CF methods were compared and the best model was selected. Smoothened data were generated with the best model for training of the ANN. The average estimation percentage errors, R_{ave}, with CF for testing were in the range of 6.332% to 0.003% when the LM type of ANN was used. Due to unsatisfactory performance of ANN after

training and testing with 21 cases, 101 cases were generated with the selected empirical model. The LM, SCG, and RB type ANN were trained with 67 cases, while the number of hidden nodes increased from 1 to 40. The performances of the ANN were evaluated by using the remaining 34 cases which they never saw before. By using trial and error method with different ANN configurations, it was decided to have the network consisting of one input layer with 5 neurons, one hidden node, and one output node.

Finally, the R_{ave} was calculated for all the ANN after 40 trials and 1000 training iterations for each cases. Table 6 showed that in case of the counter flow, the best estimations were obtained when the hidden nodes were selected 8, 10, and 34 with the LM, RB, and SCG type ANN when the LMTD method were used respectively. The LM gave the best estimations in all the cases. For the counter flow the most accurate U value estimations were obtained with the LMTD method when 8 hidden nodes were used according to tab. 6. According to tab. 7, for the counter flow the best estimations were obtained when the hidden nodes were selected 19, 7, and 37 with the LM, RB, and SCG type ANN when the LMTD method were used, respectively.

Table 6. Average estimation errors of *U* during counter flow with LM, RB, and SCG type ANN

Hidden nodes	LM [%]		Hidden nodes	SCG [%]		Hidden nodes	RB [%]	
	Training	Testing		Training	Testing		Training	Testing
6	0.000551	0.000782	8	0.005562	0.006034	32	0.052081	0.060628
7	0.000151	0.000223	9	0.003698	0.004322	33	0.071212	0.068304
8*	0.0001771	0.000121	10*	0.002583	0.002664	34*	0.041575	0.043573
9	0.000212	0.000373	11	0.009559	0.010338	35	0.10671	0.11832
10	0.000241	0.000564	12	0.009125	0.010833	36	0.15567	0.16574

* Best result

Table 7. Average estimation errors of U during parallel flow with LM, RB, and SCG type ANN

Hidden nodes	LM [%]		Hidden nodes	SCG [%]		Hidden nodes	RB [%]	
	Training	Testing		Training	Testing		Training	Testing
17	0.00070805	0.0015117	5	0.003944	0.004041	35	0.16044	0.17488
18	0.00023498	0.00034189	6	0.019334	0.021156	36	0.13307	0.15055
19*	0.00022498	0.00013071	7*	0.00217	0.002512	37*	0.027766	0.031096
20	0.00025861	0.00035	8	0.012609	0.014893	38	0.10287	0.10698
21	0.00011526	0.00018744	9	0.012872	0.014098	39	0.16836	0.19903

* Best result

For compact representation and consistency, the LM type ANN with 8 nodes was selected. The R_{ave} value was 0.000121% which means that the LM type ANN was capable to learn at high accuracy. The R-square error, R^2, for the training, the testing, and the validation was 1 when the LM type ANN for counter flow and parallel flows were trained. Furthermore, ANOVA was employed to determine differences between the predicted U for 21 cases without CF, 21 cases with CF, and the genarated 101 cases. The F-statistic was $F = 0.0044$ ($p = 0.9473$) when 21 cases without CF and with CF were used. The F-statistic was $F = 0.0051$ ($p = 0.9431$) when 21 cases without CF and generated 101 cases were used. The F-statistic was $F = 3.36e{-}4$ ($p = 0.9854$) when 21 cases with CF and generated 101 cases were used. The F-statistic was 0.003 ($p = 0.997$ when all cases were used.) The F-statistic for all cases indicated that all groups have no significant difference. All type of test indicate that the generated 101 cases have more

accuracy than 21 cases without CF and with CF. For the counter flow mode, the predictions of the ANN were compared with the experimental results in fig. 3. The estimations were very close to the experimental data. According to the generated U (U_g) and the predicted U (U_p), the 3-D plot in fig. 4 illustrated the U prediction performance of the LM type ANN respect to three inputs: the temperatures of the water at the entrance, at the outlet, and the mass-flow rate of water. For the counter flow, the maximum value of U was obtained with LMTD method was 369.23, fig. 4.

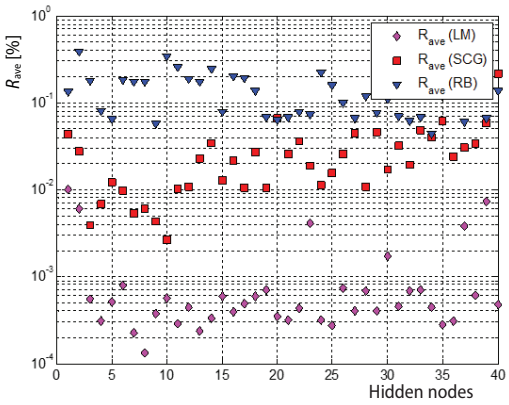

Figure 3. Comparison of R_{ave} error for LM, RB, and SCB testing data

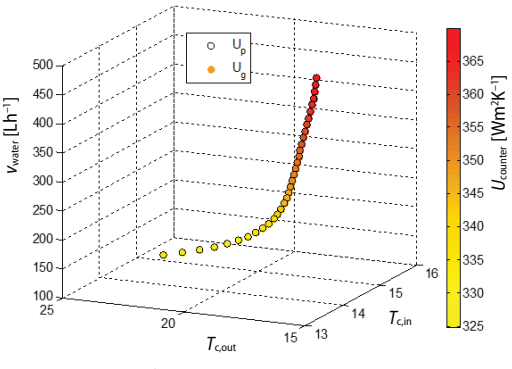

Figure 4. The 4-D Plot out of U for LM algorithm

Conclusions

In the paper, CF and ANN combination was proposed to represent the experimental data when only limited number of readings is available. The curve fitting increased the data points with the help of the selected empirical model without creating extreme deviations between the data typically observed at the estimations of over fitted ANN models.

- In the study, empirical equations were used to smoothen the experimental data and to increase of the cases for the training and testing data. The performances of the empirical equations varied from case to case. The prediction of the LM, RB, and SCG type ANN, which were trained and tested by using the generated data, were compared when the LMTD method were used respectively. The results have been discussed in term of astimating errors. The LM type ANN gave the minimum estimation errors.
- The results indicated that CF and LM type ANN combination may be used to represent the experimental data when limited number of test points were obtained experimentally. The performances of the curve fitting methods were very close to each other in the considered cases, and any of them could be used to smoothen the data and to generate training and test cases for the ANN.

Nomenclature

A_s – heat transmission area, [m^2]
i – iteration number
m – independent variable
N – number of data
p – constant value
$\dot{Q}_e$ – heat transfer rate emitted from hot liquid, [W]
R – a function of independent variables
R^2 – adjusted R-squared
R_{ave} – average percentage error, [%]
T – temperature, [ºC]

ΔT – temperatures differences, [ºC]
U – overall heat transfer coefficient, [$Wm^{-2}K^{-1}$]

Subscripts and superscripts

c – cold
e – experimental
g – generated
h – hot
in – inlet
m – mean
n – number of term in the series
out – outlet
p – predicted

Acronyms

ANN – artificial neural network
CF – curve fitting
HX – heat exchanger
LM – Levenberg Marquart
LMTD – logarithmic mean temperature difference
min – minimum
mH_2O – meter of water coloumn
NTC – negative temperature coefficient
PID – proportional + integral + derivative
PT100 – temperature sensor
RB – resilient backpropagation
RTD – resistance temperature detector
SCG – scaled conjugate gradient
SSR – solid state relay
SV – solenoid valve

References

[1] Shah, R. K., Seculic, D. P., *Fundamentals of Heat Exchanger Design*, John Wiley and Sons, Inc., Hoboken, New Jersey, USA, 2003
[2] Cengel, Y. A., *Heat and Mass Transfer*, McGraw-Hill, New York, USA, 2007
[3] Holman, J. P., *Heat Transfer*, McGraw-Hill, New York, USA, 2010
[4] Patrascioiu, C., Radulescu, S., Modeling and Simulation of the Double Tube Heat Exchanger Case Studies, in. *Advances in Fluid Mechanics & Heat & Mass Transfer*, (Eds. Mastny, P., Perminov, V.,), WSEAS Press, Istanbul, Turkey, 2012, pp. 35-41
[5] Islamoglu, Y., A New Approach for the Prediction of the Heat Transfer Rate of the Wire-On-Tube Type Heat Exchanger-Use of an Artificial Neural Network Model, *Applied Thermal Engineering*, *23* (2003), 2, pp. 243-249
[6] Islamoglu, Y., Kurt, A., Heat Transfer Analysis Using ANNs with Experimental Data for Air Flowing in Corrugated Channels, *Int. Journal Heat Mass Transfer*, *47* (2004), 6-7, pp. 1361-1365
[7] Pacheco-Vega, A*., et al.*, Neural Network Analysis of Fin-Tube Refrigerating Heat Exchanger with Limited Experimental Data, *Int. Journal Heat and Mass Transfer*, *44* (2001), 5, pp. 763-770
[8] Mohanraj, M., *et al.*, Applications of Artificial Neural Networks for Thermal Analysis of Heat Exchangers – A Review, *International Journal of Thermal Sciences, 90* (2015), Apr., pp. 150-172
[9] Diaz, G., *et al.,* Dynamic Prediction and Control of Heat Exchangers Using Artificial Neural Networks, *Int. Heat and Mass Transfer*, *44* (2001), 9, pp. 1671-1679
[10] Esfe, M. H., Designing a Neural Network for Predicting the Heat Transfer and Pressure Drop Characteristics of Ag/Water Nanofluids in a Heat Exchanger, *Applied Thermal Engineering, 126* (2017), 5, pp. 559-565
[11] Naphon, P., *et al.*, Artificial Neural Network Analysis on the Heat Transfer and Friction Factor of the Double Tube with Spring Insert, *Int. J. Applied Engineering Research, 11* (2016), 5, pp. 3542-3549
[12] Fadare, D. A., Fatona, A. S., Artificial Neural Network Modeling of Heat Transfer in a Staggered Cross-Flow Tube-Type Heat Exchanger, *The Pacific Journal of Science and Technology*, *9* (2008), 2, pp. 317-323
[13] Islamoglu, Y., Performance Prediction for Non-Adiabatic Capillary Tube Suction-Line Heat Exchanger: An Artificial Neural Network Approach, *Energy Conversion and Management*, *46* (2005), 2, pp. 223-232
[14] Shabiulla, A. M., Sivaprakasam, S., Experimental Investigation and Neural Modeling of Water-Butanol System in a Spiral Plate Heat Exchanger, *Int. J. Application or Innovation in Engineering, 2* (2013), 9, pp. 125-135
[15] Xie, G. N., *et al.*, Heat Transfer Analysis for Shell-And-Tube Heat Exchangers with Experimental Data by Artificial Neural Networks Approach, *Applied Thermal Engineering*, *27* (2007), 5-6, pp. 1096-1104
[16] Colorado, D., *et al.*, Heat Transfer Using a Correlation by Neural Network for Natural Convection from Vertical Helical Coil in Oil and Glycerol/Water Solution*, Energy*, *36* (2011), 2, pp. 854-863
[17] Patra, S. R., *et al.*, Artificial Neural Network Model for Intermediate Heat Exchanger of Nuclear Reactor, *Int. J. Computer Applications, 1* (2010), 26, pp. 63-69
[18] Erdogan, A., Colpan, C. O., Performance Assessment of Shell and Tube Heat Exchanger Based Subcritical and Supercritical Organic Rankine Cycles, *Thermal Science*, *22* (2018), Suppl. 3, pp. S855-S866

[19] Ali, M., *et al.*, Parametric Investigation of a Counter-Flow Heat and Mass Exchanger Based on Maisotsenko Cycle, *Thermal Science*, *22* (2018), 6B, pp. 3099-3106
[20] Direk, M., and Kelesoglu, A., Automotive Air Conditioning System with an Internal Heat Exchanger Using R1234YF and Different Evaporation and Condensation Temperatures, *Thermal Science*, *23* (2019), 2B, pp. 1115-1125
[21] Yang, W., *et al.*, Two-Region Simulation Model of Vertical U-Tube Ground Heat Exchanger and its Experimental Verification, *Applied Energy*, *86* (2009), 10, pp. 2005-2012
[22] Hosseini, M. J., *et al.*, A Combined Experimental and Computational Study on the Melting Behavior of a Medium Temperature Phase Change Storage Material Inside Shell and Tube Heat Exchanger, *International Communications in Heat and Mass Transfer*, *39* (2012), 9, pp. 1416-1424
[23] Jamali, A., *et al.*, Optimization of a Novel Carbon Dioxide Cogeneration System Using Artificial Neural Network and Multi-Objective Genetic Algorithm, *Applied Thermal Engineering*, *64* (2014), 1-2, pp. 293-306
[24] Seber, A. F., Wild, C. J., *Nonlinear Regression*, John Wiley and Sons, Inc., New Jersey, USA, 2003
[25] Haykin, S., *Neural Networks and learning Machines*, Pearson Education Inc., New Jersey, USA, 2009
[26] Kocyigit, N., Fault and Sensor Error Diagnostic Strategies for a Vapor Compression Refrigeration System by Using Fuzzy Inference Systems and Artificial Neural Network, *Int. J. Refrigeration*, *50* (2015), Feb., pp. 69-79
[27] ***, Danfos Heat exchangers, http://files.danfoss.com/technicalinfo/dila/01/DKRCC.PD.FD0.A8.02.pdf E-book
[28] Barbeau, E. J., *Polynomials*, Springer, New York, USA, 2003
[29] ***, MathWorks, https://www.mathworks.com/help/stats/anova1.html
[30] Mohanraj, M., *et al.*, Applications of Artificial Neural Networks for Refrigeration, Air Conditioning and Heat Pump Systems, *Renewable and Sustainable Energy Reviews, 16* (2012), 2, pp. 1340-1358
[31] Hosoz, M., *et. al*, An Adaptive Neuro-Fuzzy Inference System Model for Predicting the Performance of a Refrigeration System with a Cooling Tower, *Expert Systems with Applications, 38* (2011), 11, pp.14148-14155

Paper submitted: December 6, 2017
Paper revised: February 28, 2018
Paper accepted: March 12, 2018